3D FINITE ELEMENT DAMAGE ANALYSIS OF A BASKET-WEAVE LAMINATE SUBJECTED TO IN-PLANE SHEAR

G. Baruffaldi, E. Riva, G. Nicoletto

Dipartimento di Ingegneria Industriale - Parco Area delle Scienze 181/A
Università di Parma, 43100 Parma, Italy

ABSTRACT

A finite element based approach to the prediction of stiffness and damage evolution in a basked weave laminate is presented. After defining the appropriate representative volume and detailed finite element mesh development, the special case of in-plane shear loading is considered. Microscopic stress and strain fields show the complex nature of woven laminate mechanics. A homogeneization procedure is used to determine macroscopic shear stress and strains. Experimental data are used then to assess the model predictions.

1. INTRODUCTION

Composite laminates are widely used in many industrial sectors. High-performance components may be composed of a stack of unidirectional (UD) laminas or of 2D woven fabric plies arranged in a sequence chosen to optimize the mechanical properties. Woven laminates are characterized by such advantages as balanced in-plane mechanical properties, improved impact resistance and easy handling and shaping. They are also increasingly cost competitive with respect to unidirectional laminated composites, [1-2].

Constituent materials for the woven reinforcement include carbon, glass and polymer; these are usually combined with a polymeric matrix. To obtain a textile preform, thousands of fibers are gathered to form yarns, which are subsequently woven according to a given pattern or texture. There are a range of different fabric patterns, such as plain weave, basket weave, twill weave, satin weave etc. The geometrical variables of the reinforcement (the yarn spacing, the yarn thickness and the weave pattern) or the fiber and resin types may be varied to reach the needed mechanical properties. Other important factors that influence the mechanical behavior of the laminate are the packing density of the yarns and the fiber volume fractions.

Compared to unidirectional laminates, the mechanics of woven composites is more complex because of the architecture of the reinforcement. Although analytical models can contribute to an enhanced understanding of these materials and are found extensively in the literature, [1-4], they have also inherent practical limitations. Therefore, computational approaches based on the finite element method have been used increasingly in the past decade to model not only the global laminate stiffness, but also damage evolution and laminate strength, [5-16]. Modeling strength is especially complex theoretically and accepted procedures have not yet been validated completely. Most works considered the plain weave architecture because of its simplicity and popularity. Recently, however, the present authors have examined the twill weave texture and compared to the plain weave case. In terms of basic loading, most studies concentrated on the in-plane in-line tensile loading for its practical relevance although complex shell structures undergo biaxial loading conditions including in-plane shear components.

The main aim of this paper is to present a computational analysis of the progressive failure in a carbon-fiber-reinforced, basket weave laminate under in-plane shear loading. First, the geometry of the basket weave architecture is examined and an RV identified. Predictions of the global stiffness and strength under in-plane shear loading conditions are discussed assessed against experimental data.

2. FINITE ELEMENT MODEL DEVELOPMENT

The mechanical response of a woven laminate can be analyzed at different length scales using different levels of homogeneization, [6]. The term homogeneization refers to the passage from the micro to the macro scale to relate the mechanical properties of the laminate to the properties of the single phases, [4, 6]. In the case of a woven laminate there are two levels of homogeneization. At the first level, each lamina can be modeled as a regular arrangement of the yarns according to a prescribed texture. Therefore, the repetitive nature of a texture can be exploited identifying a representative volume, RV (also termed unit cell), as the building block of the lamina. The macroscopic mechanical response of a lamina is then obtained starting from the mechanical properties of yarn and matrix. At the second level, characterized by a smaller length scale, the yarn itself is modeled as a regular assembly of fibers in a polymeric matrix and the macroscopic mechanical properties of the yarn can be estimated starting from the properties of the fibers and matrix and the fiber volume fraction. Here only the first level of homogeneization is considered and discussed in detail.
The application of the finite element approach to the prediction of material behavior is divided into the following steps:

- Identification of the RV of the woven composite
- Finite element mesh generation for the RV
- Definition of boundary conditions applied to the RV
- Definition of material constitutive laws and application of damage models.

2.1 IDENTIFICATION OF THE REPRESENTATIVE VOLUME

Woven laminas are obtained by interlacing yarns in two mutually orthogonal (warp and fill) directions according to a variety of possible weave patterns. The repetitive nature of these patterns suggests the identification of a representative volume (RV) as the ideal building block of the lamina, and of the laminate, by multiplication in the different spatial directions. Apparently, each weave patterns has its RV: the basket weave, which has two warp yarns that interlace over and under two fill yarns, is considered in this work and the corresponding RV is outlined in figure 1.

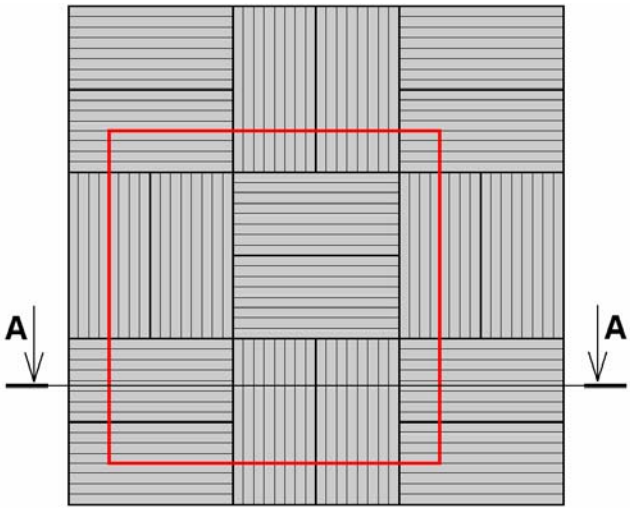

"**Fig. 1.** Basket-weave texture and related RV"

The cross-sectional view of the lamina is presented in figure 2 to help in defining geometrical parameters and discussing modeling issues and simplifying assumptions. Geometrical parameters related to the material structure are defined in figure 2. They are the yarn thickness b, the lamina thickness $2b$, the yarn width a, the yarn-to-yarn gap g, the length of the straight portion of the yarn $c = a+g$. The yarn cross section is assumed to be defined by two circular arcs having the radius of curvature R_f. The crimped portion of the warp yarn has a radius of

curvature, R_t. Figure 2 shows also that the matrix envelops the yarn fibers and fills the voids at the edges of the yarn intersections.

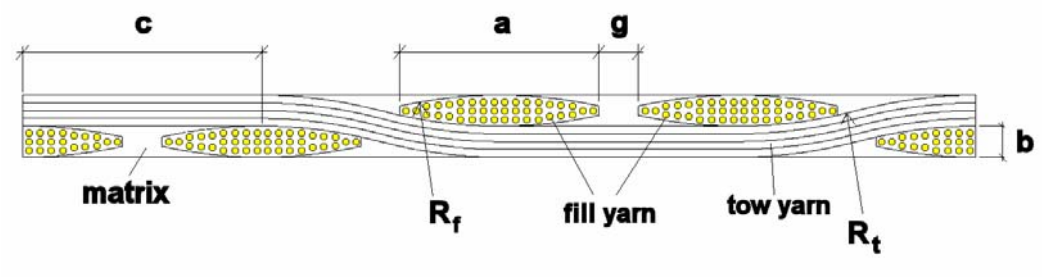

"**Fig. 2.** Cross sectional view of the basket weave (section A-A)".

The geometrical model of the RV is parametric for flexible application to different practical cases. However, sectioning, polishing and microscopic inspection of an actual eight-ply, basket-weave laminate was used to determine realistic values of the structural parameters. The total laminate thickness was 2.4 mm. Yarns were made of 3k 7-μm-dia. carbon fibers and were identical in the warp and the fill directions. The fiber volume fraction V_f = 42%. The architectural parameters used in the finite element model are given in Table 1.

"**Table 1**. Parameters characterizing the basket-weave geometry "
(Variables are defined in Fig. 1b - Dimensions in mm)

a	b	c=a+g	g	R_L	R_T
1.789	0.172	2.042	0.253	6.147	6.113

2.2 FINITE ELEMENT MESH GENERATION OF THE RV

A commercial solid modeling software, (I-DEAS SDRC), was used to generate a parametric 3D model of the interlaced yarn structure. The specific RV for the basket weave texture shown in figure 1 was meshed using brick and wedge solid elements. The tight ply packing of composite laminate suggested to assume that warp and fill yarns in this model share some nodes where they closely overlap. Adjacent yarns are separated by gap filled with resin as shown in figure 3a. Convergence studies were performed to define the optimized mesh shown in figure 3, which is characterized by 73728 solid element and 75595 nodes. The yarns were meshed first; the matrix was then defined by filling the remaining volumes as shown in figure 3b.

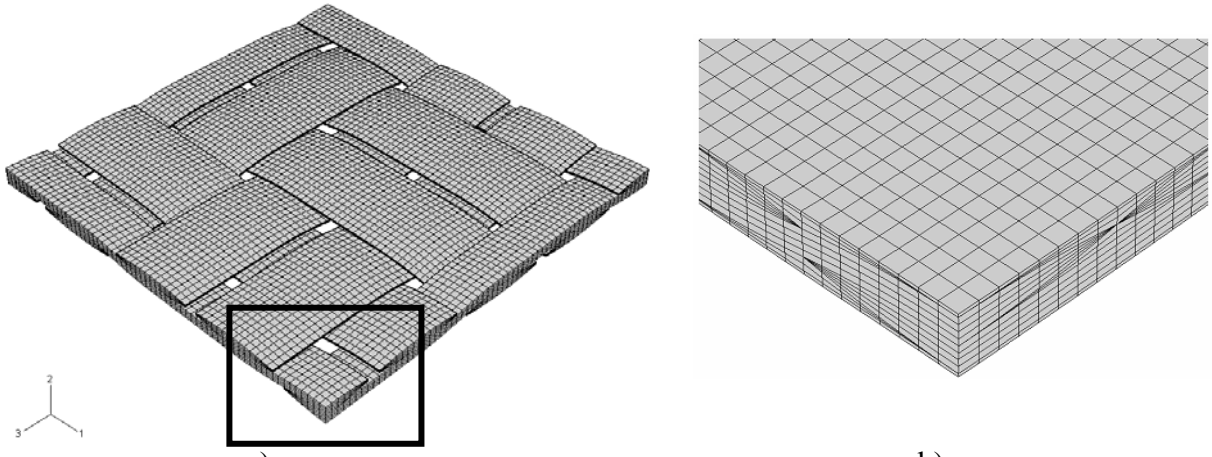

a) b)

"**Fig. 3** a) 3D Finite element model of the warp and fill yarns
b) yarn and filling matrix ".

2.3 BOUNDARY CONDITIONS FOR THE RV

Appropriate boundary conditions must be applied to the RV model to simulate the presence of the adjacent RV in the same plane (for a single lamina) and of other RV positioned above and below (for a thick laminate).

Finite element modeling with a displacement formulation requires the specification of boundary conditions that generate local (microscopic) stress and strain fulfilling the periodicity of the heterogeneous material. Therefore, the displacement fields $\underline{u}(\underline{x})$ inside the RV is assumed to be related to the strain fields by the following general equation, [17], see Suquet (1985),:

$$\underline{u}(\underline{x}) = \underline{u}^{o} + \underline{\underline{\Omega}}\,\underline{x} + \underline{\underline{E}}\,\underline{x} + \tilde{\underline{u}}(\underline{x}) \tag{1}$$

Where the first two terms, $\underline{u}^{o}$ and $\underline{\underline{\Omega}}$, are rigid body displacement and rotation of the RV, respectively, $\underline{\underline{E}}$ the macroscopic homogenous strain on RV and $\tilde{\underline{u}}(\underline{x})$ is the periodic part of the displacement field, which is associated to a periodic strain with zero average value.

The approach of [6] using nodes A, B, C, D and F in figure 4 in the center of the lateral sides S_a, S_b, S_c and S_d, was used to apply the displacement boundary conditions in accordance to Eq. 1.

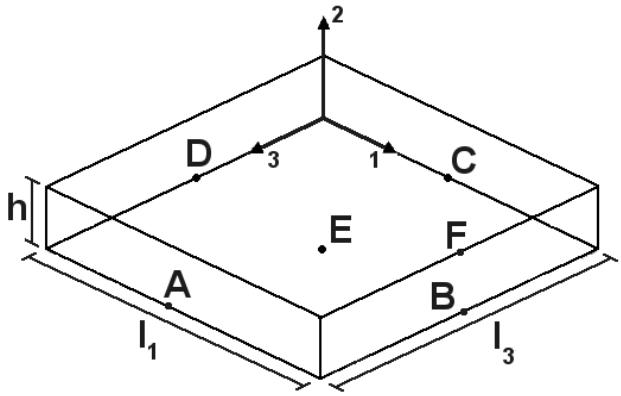

"**Fig. 4** Reference points on the finite element model."

The following equations were preliminarily defined so that all corresponding nodes on the opposite sides behave like the mid reference nodes:

$$\underline{u}^{A} - \underline{u}^{C} = \underline{u}^{L} - \underline{u}^{M} \tag{2}$$

$$\underline{u}^{B} - \underline{u}^{D} = \underline{u}^{J} - \underline{u}^{K} \tag{3}$$

$$\underline{u}^{F} - \underline{u}^{B} = \underline{u}^{P} - \underline{u}^{Q} \tag{4}$$

where *L* and *M* are corresponding nodes on opposite sides defined by $x_3 = l_3$ e $x_3 = 0$
J and *K* are corresponding nodes on opposite sides defined by $x_1 = l_1$ e $x_1 = 0$
P and Q are corresponding nodes on opposite sides defined by $x_2 = h$ e $x_2 = 0$

Eqs. (2), (3), (4) simulate the presence of other RVs in the 1, 2 and 3 coordinate directions. Since in this paper the single lamina case is studied, Eq. (4) is not applied. An additional reference node, E, is identified in the middle of the $x_2 = 0$ side of the RV. To prevent rigid body motions of the model, this node is fully restrained by imposing $\underline{u}^{0} = \underline{0}$. Rigid rotations about the 1, 2 and 3 axes are also eliminated imposing the following equations:

$$\frac{l_3}{l_1} u_3^{B} - \frac{l_3}{l_1} u_3^{D} + u_1^{C} - u_1^{A} = 0 \tag{5}$$

$$\frac{l_1}{h}u_3^F - \frac{l_1}{h}u_3^B + u_2^A - u_2^C = 0 \tag{6}$$

$$\frac{l_3}{h}u_1^F - \frac{l_3}{h}u_1^B + u_2^D - u_2^B = 0 \tag{7}$$

where l_1, l_3 and h are defined in figure 4.
The approach using reference nodes on the sides of the RV facilitates the application of the different basic modes of loading. In this work in-plane shear was applied to the RV simply enforcing u_1 displacement components of equal magnitude but opposite sign to the reference points A e C, see figure 4. The present finite element analysis is nonlinear as an elastic-plastic behavior of the matrix is assumed and the damage initiation and evolution is considered. Therefore, the boundary is displaced incrementally and the microscopic stress and strain fields ($\underline{\underline{\sigma}}(\underline{x})$, $\underline{\underline{\varepsilon}}(\underline{x})$) are determined at the end of each time increment. A following homogeneization procedure is applied to determine the macroscopic stresses and strain ($\underline{\underline{\Sigma}}$, $\underline{\underline{E}}$), representative of the laminate response: the macroscopic stress $\underline{\underline{\Sigma}}$ is obtained according to the following integral:

$$\underline{\underline{\Sigma}} = \frac{1}{V}\int_V \underline{\underline{\sigma}}\, dV \tag{8}$$

The corresponding macroscopic strains are determined from the displacement components of the reference nodes as follows:

$$E_{11} = \frac{u_1^B - u_1^D}{l_1} \tag{9a}$$

$$E_{22} = \frac{u_2^F - u_2^B}{h} \tag{9b}$$

$$E_{33} = \frac{u_3^A - u_3^C}{l_3} \tag{9c}$$

$$E_{13} = \frac{u_1^A - u_1^C}{l_3} \tag{9d}$$

$$E_{12} = \frac{u_2^B - u_2^D}{l_1} \tag{9e}$$

$$E_{23} = \frac{u_2^A - u_2^C}{l_3} \tag{9f}$$

2.4 MATERIAL AND DAMAGE MODELS

In the woven lamina, tow and fill yarns are arranged according to the basket weave architecture while reinforcement fibers are arranged unidirectionally within each yarn, figure 1. Therefore, yarns were treated macroscopically as transversely isotropic homogeneous materials. The elastic moduli and strength properties used in the present calculations are listed in Table 2 and Table 3, where the subscript 1 denotes the direction tangent to the fiber yarn axis and subscripts 2 and 3 are orthogonal to the yarn axis.
The matrix is normally a polymer and has an important role in the shear response of woven laminates, [18]. The matrix material was assumed homogeneous and isotropic with an elastic-plastic stress-strain response defined point-by-point. Some basic properties of the matrix are listed in Table 4.

"**Table 2.** Elastic moduli of the fiber yarn, [19]."

E_{11} [GPa]	E_{22} [GPa]	E_{33} [GPa]	G_{12} [GPa]	G_{13} [GPa]	G_{23} [GPa]	ν_{12}	ν_{13}	ν_{23}
151	10.1	10.1	5.70	5.70	3.40	0.24	0.24	0.5

Table 3. Strength properties of the fiber yarn, [19]."

σ_{RT11} [MPa]	σ_{RT22} [MPa]	σ_{RT33} [MPa]	τ_{R12} [MPa]	τ_{R13} [MPa]	τ_{R23} [MPa]	σ_{RC11} [MPa]	σ_{RC22} [MPa]	σ_{RC33} [MPa]
2550	152	152	97	97	55	2000	206	206

"**Table 4.** Mechanical properties of the matrix [18]."

E [MPa]	ν	σ_R [MPa]
4811	0.34	167

The progressive failure computational approach, [5], used previously to model a plain-weave textile composite from the same material system, [8], is adopted. A approach basically consists of a stress analysis and a failure analysis on an element-by-element basis. This kind of analysis facilitates the study of damage mechanisms, including failure initiation, propagation and ultimate fracture under different failure modes of a lamina and laminate. Distinct criteria were adopted for the matrix and the fiber yarn. The matrix was assumed to fail isotropically according to the maximum stress failure criterion. The damage modes of the fiber yarns were considered influenced by the material anisotropy. Therefore, considering direction 1 the local fiber direction of the yarn and directions 2 and 3 the local transverse directions of the yarn, then normal stress S11 was associated to fiber fracture while normal stresses S22 and S33 were associated to transverse matrix cracking of the yarn. Shear stresses S12, S13 and S23 controlled shear cracking of the yarn. The initial stiffnesses and ultimate strengths of the yarn are given in Tab. 2 and 3, respectively.

"**Table 5.** Failure criteria and degradation scheme for yarn material, [19]."

Failure mode	Failure condition	Discount coefficient					
		d_1	d_2	d_3	d_{23}	d_{13}	d_{12}
Longitudinal tension (σ_{T11})	$\sigma_{T1\,1} > \sigma_{RT11}$	0.01	0.01	0.01	0.01	0.01	0.01
Longitudinal compression (σ_{C11})	$\sigma_{C11} > \sigma_{RC11}$	0.01	0.01	0.01	0.01	0.01	0.01
Transverse tension (σ_{T22})	$\sigma_{T22} > \sigma_{RT22}$	1.0	0.01	1.0	1.0	0.2	0.2
Transverse compression (σ_{C22})	$\sigma_{C11} > \sigma_{RC11}$	1.0	0.01	1.0	1.0	0.2	0.2
Trasverse tension (σ_{T33})	$\sigma_{T33} > \sigma_{RT33}$	1.0	1.0	0.01	1.0	0.2	0.2
Transverse compressione (σ_{C33})	$\sigma_{C11} > \sigma_{CT11}$	1.0	1.0	0.01	1.0	0.2	0.2
Out-of plane shear (τ_{23})	$\lvert\tau_{23}\rvert > \tau_{R23}$	1.0	0.01	0.01	0.01	0.01	0.01
In-plane shear (τ_{13})	$\lvert\tau_{13}\rvert > \tau_{R13}$	1.0	1.0	0.01	1.0	0.01	1.0
Out-of-plane shear (τ_{12})	$\lvert\tau_{12}\rvert > \tau_{R12}$	1.0	0.01	1.0	1.0	1.0	0.01

In the computational procedure of damage simulation, each integration point of every finite element of the model is considered in turn and the local constitutive material law discounted by an appropriate amount, see Table 5, if a directional failure criterion (i.e. when the stress/strength ratio is equal to 1) is verified. Stresses and strains are then recalculated to determine any additional damage as a result of stress redistributions at the same load. The ultimate load is reached when the laminate cannot sustain any additional load.

3. RESULTS AND DISCUSSION

The results of the finite element analysis of the basket-weave lamina are presented in terms of modelling issues, elastic properties of the lamina and its global non-linear behavior. An initial comparison of the analytical results to experimental results is also performed.
The top view of the deformed mesh is shown in figure 5 to gain an insight into the mechanism of deformation imposed to the RV model by the periodic boundary conditions. It is apparent that the deformed model is subjected a macroscopic shear strain, whose average magnitude is controlled by the average tangential displacement component. The local mesh oscillations of the RV edges in figure 5 demonstrate also the presence of a periodic shear strain oscillation at the microscopic level, consistently with the periodicity in the boundary conditions of Eq. (1). Therefore, shear strain is nonuniform within the RV and local stress and strain concentrations result in damage localization.

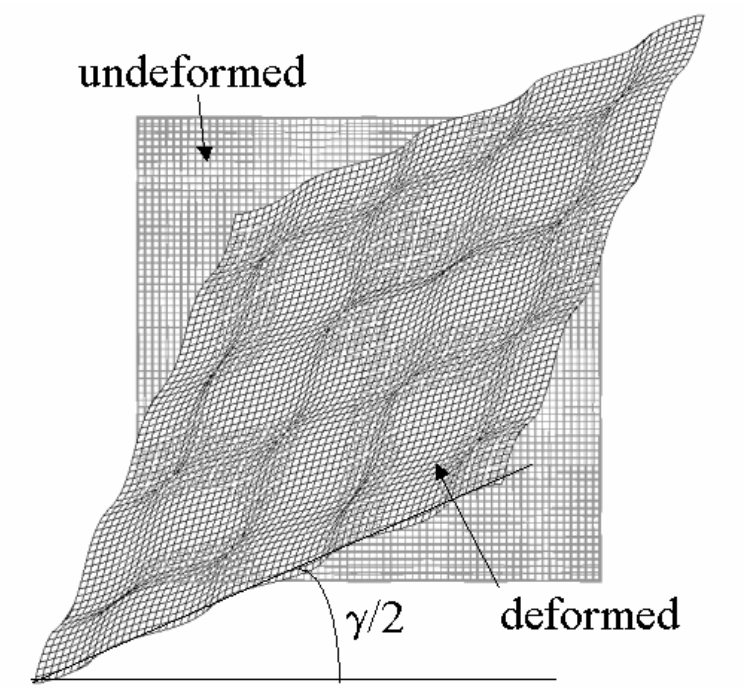

"**Fig. 5** Undeformed and deformed finite element mesh with definition of macroscopic shear strain (note that deformation is exaggerated for clarity)."

The degree of nonuniformity in the stresses and strains is obtained by appropriate mapping of the microscopic variables. The contour plot of the in-plane shear stress (i.e. S13) in the woven yarns is shown in figure 6. The influence of the yarn architecture, see Fig. 1a, is visible in the shear stress map, with shear stress distributions symmetrical with respect to the zero value within the model. Furthermore, the stress pattern is modulated by the weave pattern with shear stress concentration initially at the yarn edges, especially where they are crimped (bent out of plane by the weave architecture). Regions of reduced stress are identified as circular areas at the center pf the yarns. They are possibly related to some direct nodal link between orthogonal yarns, where they directly superpose. This modeling feature is thought to stiffen the computed RV response and is currently removed by inserting a thin layer of matrix elements.

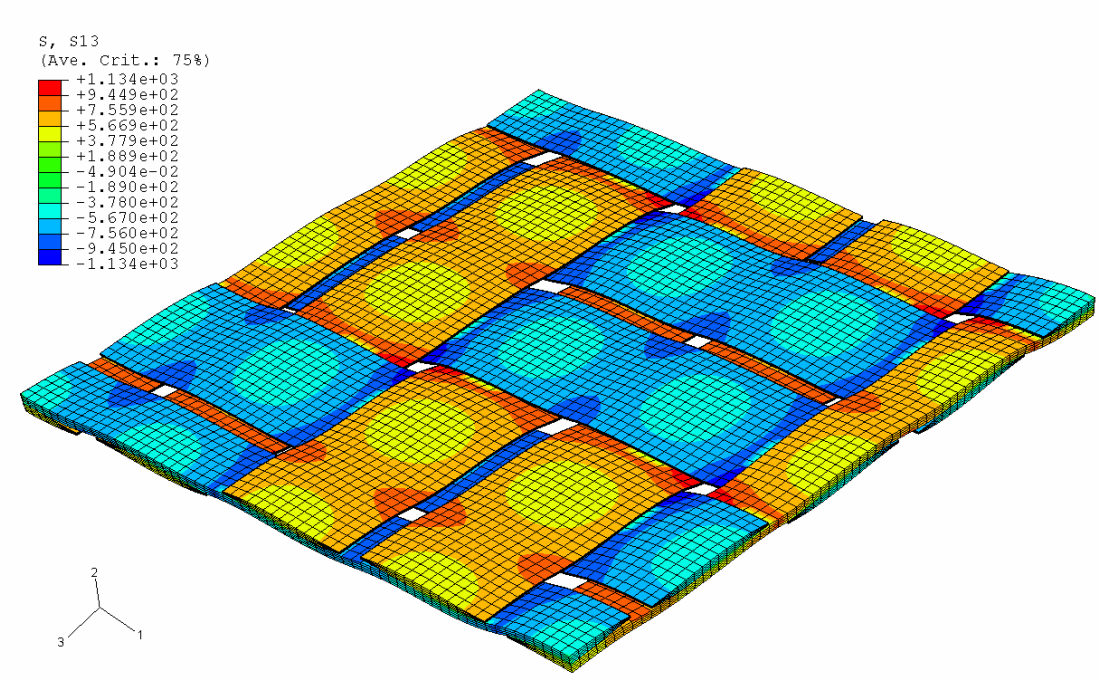

"**Fig. 6** In-plane shear stress distribution".

Table 6 compares the predicted elastic modulus in shear with previous experimental data, [20], obtained on woven composite laminates by two alterntive techniques, namely the ± 45° off-axis test and the rail shear test. The comparison is considered satisfactorely because the predicted value falls in the range defined by the two experimental techniques. As expected, the shear elastic modulus is in absolute terms greater than the shear elastic modulus of the matrix, due to the yarn stiffening effect.

"**Table 6.** Predicted elastic modulus in shear G_{13} vs. experimental data, [20]."

FEM [MPa]	± 45° off axis test [MPa]	Rail shear test [MPa]
3707	4216 (±216)	3430 (±26)

The current level of the modeling approach is best assessed comparing directly the computed shear stress vs. shear strain response, obtained with the present model, and the experimental curves as shown in figure 7. The experimental curves consistently show that, after a limited initial linear response, a woven laminate deforms according to a markedly nonlinear response. The tangent shear modulus gradually drops, possibly due to yarn rotation. The shear moduli of elasticity of Tab. 6 are given by the initial slope of the stress-strain curves.

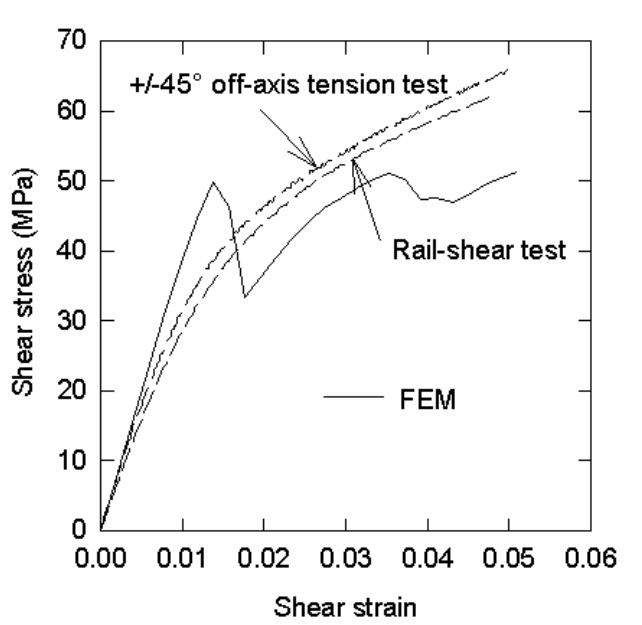

"**Fig. 7** Comparison of experimental and predicted shear stress vs. shear strain curves".

On the othern hand, the prediction of the finite element model shows in figure 7 a stiff, and almost linear, response up to 50 MPa. Then, an oscillatory trend, typical of a displacement-controlled test condition of brittle materials, where localized material failure produces a drop in stress level, is determined. Interestingly however, the trend in the predicted slope following the stress drops is similar to the experimental trends. Although the results demonstrate the potential of the approach, a number of modeling issues that need clarification are currently in the works.

4. CONCLUSIONS

The paper presented a FEM-based approach to the prediction of stiffness and damage evolution in a basked-weave lamina. The representative volume of the weave was identified and periodic boundary conditions applied to impose macroscopic in-plane shear loading conditions. Microscopic stress and strain fields showed the complex nature of woven laminate mechanics. A homogeneization procedure is used to determine macroscopic shear stress and strains. Experimental data are used then to assess the model predictions. While the predicted stiffness in shear is accurate, the global shear stress-shear strain behavior up tu failure signals the need of some further model refinement.

ACKNOWLEDGEMENT

The valuable contribution of Stefano Lazzarotti to model development and assessment in the course of his thesis work in Mechanical Engineering is acknowledged.

REFERENCES

1. **Chou T.W.**, **Ko F.K.**, Textile Structural Composites, Elsevier, New York, 1989.
2. **Naik N.K.**, Woven Fabric Composites, Tecnomic Publishing, 1994.
3. **Naik RA.**, "Failure analysis of woven and braided fabric reinforced composites", *J. Composite Materials,* Vol. 29, No. 17, 1995, 2334-63

4. **Dasgupta A.**, **Bhandarkar SM.**, “Effective thermomechanical behavior of plain-weave fabric-reinforced composites using homogeneization theory”, *Trans ASME J Eng Mater Tech,* Vol. 16, 1994, 99-105.
5. **Blackketter D.**, **Walrath D.**, **Hansen A.**, “Modeling Damage in a Plain Weave Fabric-Reinforced Composite Material”, *Journal. of Composites Technology & Research*, Vol. 15, No. 2, 1993, 136-42.
6. **Carvelli V.**, **Poggi C.**, "A Homogeneization Procedure for the Numerical Analysis of Woven Fabric Composites", *Composites: Part A*, Vol. 33, 2001, 1425-32.
7. **Chapman C.**, **Whitcomb J.**, “Effect of assumed tow architecture on predicted moduli and stresses in plain weave composites”, *J Composite Materials,* Vol. 29, No. 16, 1995, 2134-59.
8. **Guagliano M.**, **Riva E.**, “Mechanical Behavior Prediction in Plain weave Composites”, *J. Strain Analysis for Engineering Design*, Vol. 36, 2001, 153-62.
9. **Hamelin P.**, **Bigaud D.**, “A numerical procedure for elasticity and failure behavior prediction of textile-reinforced composite materials”, *J Thermoplastic Compos Mater*12, 1999, 1428-42.
10. **Nicoletto G.**, **Riva E.**, “Failure mechanisms in twill weave laminates: FEM predictions vs. experiments”, *Compoites Part A*, 2004, In press.
11. **Tan P.**, **Long L.**, **Steven GP.**, “A flexible 3D FEA modeling approach for predicting the mechanical properties of plain weave unit cell”, *Proc ICCM-11,* Gold Coast, Queensland, Australia, July 14-18, 1997.
12. **Whitcomb J. D.**, **Srirengan K.**, “Effect of Various Approximations on Predicted Progressive Failure in Plain weave Composites“, *Composite Structures*, Vol.34, 1996, 13-20.
13. **Woo K.**, **Whitcomb J.**, "Three-dimensional failure analysis of plain weave textile composites using a global/local finite element method", *J. Composite Materials*, Vol. 30, N. 9, 1996, 984-1003.
14. **Whitcomb J.**, **Kondagunta G.**, **Woo K.**, “Boundary effects in woven composites”, *J Composite Materials,* Vol. 29, No. 4, 1995, 507-24. ,
15. **Woo K.**, **Whitcomb J.**, "Global/local finite element analysis for textile composites", *Journal of Composite Materials*, Vol. 28, N. 14, 1994, 1305-21.
16. **Zako M.**, **Uetsuji Y.**, **Kurashiki T.**, “Finite element analysis of damaged woven fabric composite materials”, *Composites Science and Technology*, Vol. 63, No. 2, 2003, 507-16.
17. **Suquet P.**, 1985, “Elements of homogeneization for inelastic solid mechanics”, In: Sanchez-Palencia E, Zaoui, A., Eds. Homogeneization techniques for composite media, Lecture Notes in Physics 272, Springer, Wien, 193-278.
18. **Tabiei A.**, **Ivanov I.**, “Materially and geometrically non-linear woven composite micro-mechanical model with failure for finite element simulations”, *InternationalJournal of Non-linear mechanics*, Vol. 39, pp. 175-188, 2004.
19. **Lazzarotti S.**, “Damage modelling in woven fabric composite laminates”, Thesis in Mechanical Engineering, 2004, University of Parma.
20. **Nicoletto G.**, **Riva E.**, ″In-plane shear response of woven fabric composite laminates″, *OIAZ*, Vol. 143, Vol 5, 1998, pp.226-229.